Cellular Physiology and Biochemistry

Cell Physiol Biochem 2018;47:330-343
DOI: 10.1159/000489810
Published online: May 17, 2018
Accepted: March 13, 2018

Original Paper

Multiple Actions of Rotenone, an Inhibitor of Mitochondrial Respiratory Chain, on Ionic Currents and Miniature End-Plate Potential in Mouse Hippocampal (mHippoE-14) Neurons

Chin-Wei Huang[a] Kao-Min Lin[b] Te-Yu Hung[c] Yao-Chung Chuang[d,e] Sheng-Nan Wu[f]

[a]Department of Neurology, National Cheng Kung University Hospital, College of Medicine, National Cheng Kung University, Tainan, [b]Department of Pediatric Neurology, Chiayi Christian Hospital, Chiayi, [c]Department of Pediatrics, Chi-Mei Medical Center, Tainan, [d]Department of Neurology and Institute for Translational Research in Biomedicine, Kaohsiung Chang Gung Memorial Hospital and Chang Gung University College of Medicine, Kaohsiung, [e]Department of Neurology, Faculty of Medicine, College of Medicine, Kaohsiung Medical University, Kaohsiung, [f]Department of Physiology, National Cheng Kung University, College of Medicine, Tainan, Taiwan

Key Words
Rotenone • Voltage-gated Na^+ current • Ca^{2+}-activated Cl^- current • ATP-sensitive K^+ channel • Miniature end-plate potential • Simulation

Abstract
Background/Aims: Rotenone (Rot) is known to suppress the activity of complex I in the mitochondrial chain reaction; however, whether this compound has effects on ion currents in neurons remains largely unexplored. ***Methods:*** With the aid of patch-clamp technology and simulation modeling, the effects of Rot on membrane ion currents present in mHippoE-14 cells were investigated. ***Results:*** Addition of Rot produced an inhibitory action on the peak amplitude of I_{Na} with an IC_{50} value of 39.3 μM; however, neither activation nor inactivation kinetics of I_{Na} was changed during cell exposure to this compound. Addition of Rot produced little or no modifications in the steady-state inactivation curve of I_{Na}. Rot increased the amplitude of Ca^{2+}-activated Cl^- current in response to membrane depolarization with an EC_{50} value of 35.4 μM; further addition of niflumic acid reversed Rot-mediated stimulation of this current. Moreover, when these cells were exposed to 10 μM Rot, a specific population of ATP-sensitive K^+ channels with a single-channel conductance of 18.1 pS was measured, despite its inability to alter single-channel conductance. Under current clamp condition, the frequency of miniature end-plate potentials in mHippoE-14 cells was significantly raised in the presence of Rot (10 μM) with no changes in their amplitude and time course of rise and decay. In simulated model of hippocampal neurons incorporated with chemical autaptic connection, increased autaptic strength to mimic the action of Rot was noted to change the bursting pattern with

Yao-Chung Chuang, MD, PhD
and Sheng-Nan Wu, MD, PhD

Department of Neurology, Chang Gung Memorial Hospital, No. 123, Dapi Road, Niaosong District, Kaohsiung (Taiwan)
E-Mail ycchuang@adm.cgmh.org.tw, snwu@mail.ncku.edu.tw

emergence of subthreshold potentials. ***Conclusions:*** The Rot effects presented herein might exert a significant action on functional activities of hippocampal neurons occurring *in vivo*.

Introduction

Rotenone (Rot) is a naturally occurring isoflavone obtained from the roots of plants belonging to the Fabaceae family (*Derris elliptica* or *Lonchocarpus*). It has been used for many years on a large scale as an insecticide or pesticide. Rot-induced animal models seem to reflect similar changes characterized by Parkinson's disease [1]. Importantly, this compound is known to be a toxin that suppresses complex I of the mitochondrial respiratory chain and inhibits NADH oxidation, thereby causing the overproduction of reactive oxygen species. It inhibits the transfer of electrons from iron-sulfur centers in CI to ubiquinone via binding to the ubiquinone binding site of complex I [2]. However, this compound appears to exert any effects on ion currents in different types of cells. For example, previous reports have shown that Rot could suppress delayed rectifier K^+ current [3] and increase ATP-sensitive K^+ current [4], large-conductance Ca^{2+}-activated K^+ (BK_{Ca}) channels [5] and TRPM2 currents [4, 6]. It has been reported to enhance NMDA-induced currents in substantia nigra dopaminergic neurons [7]. A current report also showed the ability of Rot to augment L-type Ca^{2+} current in A7r5 aortic smooth myocytes [8]. However, to our knowledge, the effects of Rot on ionic currents or membrane potential in neurons still remain largely unknown.

The mHippoE-14 hippocampal cell line is known to possess the characteristics of embryonic hippocampal neurons and enables accurate in-vitro assays for use in the discovery, development and validation of new therapeutics targeted to central nervous system diseases and disorders, including obesity, stress, reproduction and metabolic disorders [9-11]. A previous report demonstrated that Rot could cause cell death in mHippoE-18 hippocampal neurons [12]. However, to our knowledge, no studies concerning the biophysical and pharmacological properties of membrane ionic currents in these cells have been thoroughly studied.

We have previously reported the biophysical and pharmacological properties of H19-7 hippocampal cell line [13, 14]. In this study, we intended to investigate the effects of Rot on ionic currents (e.g., voltage-gated Na^+ current [I_{Na}], Ca^{2+}-activated Cl^- current [$I_{Cl(Ca)}$], and ATP-sensitive K^+ [K_{ATP}] channel) and miniature end-plate potentials (MEPPs) in mHippoE-14 hippocampal neurons.

Materials and Methods

Drugs and solutions

4, 4'-Dithiodipyridine, MK-801 (dizocilpine), niflumic acid, nimodipine, rotenone (Rot, $C_{23}H_{22}O_6$), tefluthrin, tetraethylammonium chloride, tolbutamide, and tetrodotoxin were obtained from Sigma-Aldrich (St. Louis, MO), and DCPIB (4-[(2-butyl-6, 7-dichloro-2-cyclopentyl-2, 3-dihydro-1-ox-1H-inden-5-yl)oxy] butanoic acid) was from Tocris (Bristol, UK). All culture media, fetal bovine serum, L-glutamine, trypsin/EDTA and penicillin-streptomycin were obtained from Invitrogen (Carlsbad, CA). The water used in this study was deionized using a Milli-Q water purification system (Millipore, Bedford, MA).

The composition of bath solution (i.e., normal Tyrode's solution) was 136.5 mM NaCl, 5.4 mM KCl, 1.8 mM $CaCl_2$, 0.53 mM $MgCl_2$, 5.5 mM glucose, and 5.5 mM HEPES-NaOH buffer, pH 7.4. For measurement of volume-sensitive Cl^- current ($I_{Cl(vol)}$), the composition of hypotonic solution (200 mOsm/L) was 86 mM NaCl, 5.4 mM KCl, 1.8 mM $CaCl_2$, 0.53 mM $MgCl_2$, 5.5 mM glucose, and 5 mM HEPES-NaOH buffer, pH 7.4. To measure K^+ currents or membrane potential, the patch pipette was filled with a solution consisting of 140 mM KCl, 1 mM $MgCl_2$, 3 mM Na_2ATP, 0.1 mM Na_2GTP, 0.1 mM EGTA, and 5 mM HEPES-KOH buffer, pH 7.2. The free Ca^{2+} concentration for this solution was estimated to be 230 nM, assuming that the residual contaminating Ca^{2+} concentration was 70 μM, and the ratiometric fura-2 measurement with an F-250 fluorescence spectrophotometer (Hitachi, Tokyo, Japan) revealed that this solution contained 234±15

nM free Ca^{2+} for three different experiments, a value sufficient for activation of $I_{Cl(Ca)}$. To record Na^+ or Cl^- currents, K^+ ions inside the pipette solution were replaced with equimolar Cs^+ ions, and pH was adjusted to 7.2 with CsOH.

Cell preparations

Embryonic mouse hippocampal cell line (mHippoE-14; CLU198) was obtained from Cedarlane CELLutions Biosystems Inc. (Burlington, Ontario, Canada) [9]. The cells were grown as a monolayer culture in 50-ml plastic culture flasks in a humidifier environment of 5% CO_2/95% air at 37 ºC. Cells were maintained at a density of 10^6/ml in 5 ml of Dulbecco's modified Eagle's medium supplemented with 10% heat-inactivated fetal bovine serum (v/v) and 2 mM L-glutamine. The medium was refreshed every 2 days to maintain a healthy cell population. The presence of neuritis and varicosities during cell preparations was often observed. The patch clamp experiments were performed 5 or 6 days after cells were subcultured (60-80% confluence).

Electrophysiological measurements

Mouse hippocampal neurons (mHippoE-14) were harvested with 1% trypsin/EDTA solution prior to each experiment and a portion of detached cells was thereafter transferred to a recording chamber mounted on the stage of a CKX-41 inverted fluorescent microscope (Olympus, Tokyo, Japan) coupled to a digital video system (DCR-TRV30; Sony, Japan) with a magnification of up to 1500×. They were immersed at room temperature (20-25 °C) in normal Tyrode's solution containing 1.8 mM $CaCl_2$. Patch pipettes were made from Kimax-51 glass capillaries (#34500; Kimble, Vineland, NJ) using a PP-830 electrode puller (Narishige, Tokyo, Japan) or a P-97 micropipette puller (Sutter, Novato, CA), and their tips were then fire-polished with an MF-83 microforge (Narishige). The recording pipettes had a resistance of 3-5 MΩ when immersed in the different solutions described above. Patch-clamp recordings were made in whole-cell, cell-attached, or inside-out configuration by means of an RK-400 amplifier (Bio-Logic, Claix, France) or an Axopatch 200B amplifier (Molecular Devices, Sunnyvale, CA) [14]. Liquid junctional potential was adjusted immediately before establishment of the seal.

Data recordings

The signals consisting of voltage and current tracings were stored online in an ASUSPRO-BU401LG computer (ASUS, Taipei City, Taiwan) at 10 kHz connected through a Digidata 1550 digitizer (Molecular Devices) which was driven by pCLAMP 10.2 software (Molecular Devices). Current signals were low-pass filtered at 3 kHz. The data achieved during each experiment were analyzed off-line using different kinds of analytical tools including LabChart 7.0 program (AD Instruments; Gerin, Tainan City, Taiwan), OriginPro 2016 (OriginLab, Northampton, MA) and custom-made macro procedures built under Microsoft Excel 2013 (Redmond, WA). Through digital-to-analogue conversion, the gapped voltage-step protocols with either rectangular or ramp pulses created from pCLAMP 10.2 were commonly employed to evaluate the steady-state activation or inactivation curve for different types of ion currents (e.g., I_{Na} and $I_{Cl(Ca)}$).

Data analyses

To determine concentration-dependent inhibition of Rot on the peak amplitude of I_{Na}, cells were bathed in Ca^{2+}-free Tyrode's solution and the depolarizing pulses from -80 to -10 mV with a duration of 30 msec at a rate of 1 Hz were applied. The peak amplitude of I_{Na} measured during cell exposure to different concentrμμations (1-300 μM) of this compound was thereafter compared with the control value. To ensure accurate fitting, the concentration-dependent relation of Rot on inhibition of I_{Na} was fit using a modified form of sigmoidal Hill equation:

$$Percentage\ inhibition\ (\%) = \frac{E_{max} \times [Rot]^{n_H}}{IC_{50}^{n_H} + [Rot]^{n_H}}$$

where [Rot] indicates the Rot concentration; IC_{50} and n_H are the concentration needed for a 50% inhibition and Hill coefficient, respectively; and E_{max} is the maximal reduction in peak I_{Na} amplitude caused by Rot.

The concentration-dependent stimulation of Rot on $I_{Cl(Ca)}$ was also determined with the use of a Hill function,

$$Percentage\ increase\ (\%) = \frac{E_{max} \times [Rot]^{n_H}}{EC_{50}^{n_H} + [Rot]^{n_H}}$$

where [Rot] is the Rot concentration, EC_{50} and n_H are half-maximal concentration of Rot required for activation of $I_{Cl(Ca)}$ and the Hill coefficient, respectively, and E_{max} is the maximal increase of $I_{Cl(Ca)}$ stimulated by Rot.

The *I-V* relationship of peak I_{Na} with or without addition of Rot was derived and fit with a Boltzmann equation given by:

$$I = \frac{G}{1+\exp\left[\frac{-(V-V_h)}{k}\right]} \cdot (V - E_{rev})$$

where V is the voltage in mV, E_{rev} the reversal potential of I_{Na} (fixed at +45 mV), G the Na^+ conductance in nS, and I the current in pA, while V_h and k are the gating parameters.

The quasi steady-state inactivation curve (i.e., h_∞-V curve) of I_{Na} in the presence or absence of Rot was plotted against the conditioning potential and fit with the following equation adapted from another Boltzmann function:

$$\frac{I}{I_{max}} = \frac{1}{1+\exp[(V-V_{1/2})/k]}$$

where I/I_{max} is the h_∞ factor, V the conditioning potential in mV, $V_{1/2}$ the membrane potential for half-maximal inactivation, and k the slope factor of inactivation curve for I_{Na}.

The amplitude of K_{ATP}- or BK_{Ca}-channel currents was analyzed using pCLAMP 10.2 (Molecular Devices). Multi-gaussian adjustments of the amplitude distributions among channels were employed to determine single-channel currents. When the single-channel amplitude was small as compared with the noise level, mean variance analysis for detection of single-channel opening event was also performed [15].

Statistical analyses

The values are expressed as the means±SEM with sample sizes (n) indicating the number of cells from which the data were taken, and error bars are plotted as SEM. By virtue of a least-squares minimization procedure, linear or nonlinear curve-fitting to the data sets was performed with the aid of Excel 2013 (i.e., Solver subroutine) or OriginPro 2016. The paired or unpaired Student's *t*-test and one-way analysis of variance with the least-significance-difference method for multiple comparisons were used for the statistical evaluation of differences among means. Non-parametric Kruskal-Wallis test was used, as the assumption of normality underlying ANOVA was violated. Statistical analyses were made using SPSS version 22.0 (IBM Corp., Armonk, NY). Statistical significance was determined at a P value of <0.05.

Computer simulations

To evaluate how autaptic changes influence the pattern of bursting firing, a theoretical model of bursting firing of action potentials (APs) was adapted from previous work [16, 17]. The XC model is based primarily on biophysical properties of hippocampal CA3 pyramidal neurons and comprises the delayed-rectifier K^+ current, the transient K^+ current, the Ca^{2+}-activated K^+ current, the Na^+ current, and the Ca^{2+} current. In the present simulations, the conductance values and reversal potentials used to solve the set of differential equations are listed in Table 1. Detailed descriptions of XC modeled neuron were provided previously [16, 17]. Moreover, a chemical autapse, which used the fast threshold modulation scheme [18, 19], was incorporated into the modeled neuron in attempts to mimic the Rot effects observed in mHippoE-14 cells. The function is described as follows:

$$I_{aut} = -g_{aut} \times [V - V_{syn}] \times S(t-\tau)$$

$$S(t-\tau) = \frac{1}{1+\exp[-k(V(t-\tau)-\theta)]}$$

Table 1. Default parametric values used for the modeling of hippocampal CA3 pyramidal neurons

Symbol	Description	Value
Cm	Membrane capacitance (pF)	1
g_{Na}	Na^+ current conductance (S/cm²)	2
g_{Ca}	Ca^{2+} current conductance (S/cm²)	5
g_{KDR}	Delayed rectifier K^+ current conductance (S/cm²)	0.08
g_A	A-type K^+ current conductance (mS/cm²)	0.1
g_{KCa}	Ca^{2+}-activated K^+ current conductance (mS/cm²)	0.4
g_{Kahp}	After-hyperpolarization K^+ current conductance (mS/cm²)	0.0018
g_{leak}	Leak current conductance (mS/cm²)	0.0167
I_{app}	Applied current (mA)	0.02
V_{Na}	Na^+ reversal potential (mV)	50
V_K	K^+ reversal potential (mV)	-91
V_{Leak}	Reversal potential for leak current (mV)	-65
V_{syn}	Reversal potential for excitatory synapse (mV)	2
τ	Autaptic delayed time (msec)	5

where g_{aut} represents autaptic self-feedback strength (conductance), I_{aut} is the autaptic current, $V(t-\tau)$ is the APs of neuron i at earlier time t-τ, τ (in unit of msec) is autaptic delayed time, and V_{syn} is the reversal potential for excitatory synapse. In the chemical synapse function embedded in the modeled neuron, the values of k and θ are arbitrarily set at 1 and 0. The ordinary differential equations were solved numerically using the explicit Euler method with a time step of 0.001 msec.

Results

Effect of Rot on voltage-gated Na^+ current (I_{Na}) in mHippoE-14 hippocampal neurons

We first investigated whether Rot has any effects on I_{Na} present in mouse hippocampal neurons. In this series of experiments, cells were bathed in Ca^{2+}-free Tyrode's solution containing 10 mM tetraethylammonium chloride and 0.5 mM $CdCl_2$ and the pipette was filled with a Cs^+-containing solution, the composition of which was described under Materials and Methods. As the cell was rapidly depolarized from -80 to -10 mV, addition of Rot (10 μM) resulted in a progressive reduction of peak I_{Na} in these cells (Fig. 1A), and Rot-sensitive I_{Na} was shown in inset of Fig. 1A. For example, when cells were exposed to 10 μM Rot, the peak amplitude of I_{Na} elicited by membrane depolarization from -80 to -10 mV was significantly diminished by 15.9±1.1 % to 2338±160 pA (n=11, P<0.05) from a control value of 2783±187 pA (n=11). Likewise, the density of peak I_{Na} was decreased from 99.4±5.8 to 83.5±4.7 pA/pF (n=11, P<0.05). After washout of this agent, peak current amplitude was partially returned to 2613±166 pA (n=7). However, neither activation nor inactivation time constants of peak I_{Na} were changed in the presence of 10 μM Rot. Moreover, neither activation nor inactivation time course of I_{Na} elicited by rapid membrane depolarization was modified as the cells were acutely exposed to Rot. As depicted in Fig. 1B, averaged *I-V* relationship of peak I_{Na} taken with or without addition of 10 μM Rot remained unaltered, despite its ability to suppress the peak amplitude of I_{Na}. The reversal potential of peak I_{Na} did not differ significantly between the absence and presence of Rot. The *I-V* curves obtained in the control and during cell exposure to 10 μM Rot were fitted with a Boltzmann equation as described in Materials and Methods. In control (i.e., in the absence of Rot), G=55.7±1.2 nS, V_h=-29.3±0.8 mV, k=8.6±0.3 (n=7), while in the presence of 10 μM Rot, G=45.1±0.9 nS, V_h=-31.1±0.8 mV, k=8.9±0.3 (n=7). The results showed that the values of neither V_h nor k was significantly changed in the presence of Rot (P>0.05), although the value of G (Na^+ conductance) was diminished (P<0.05). Moreover, in the continued presence of Rot, subsequent addition of tefluthrin (10 μM) significantly reversed Rot-induced decrease of peak I_{Na} (Fig. 1D). Tefluthrin is a pyrethroid insecticide known to activate I_{Na} [20, 21].

The effect of Rot on the steady-state inactivation of I_{Na} recorded from mHippoE-14 cells was also determined. In this set of experiments, cells were bathed in Ca^{2+}-free, Tyrode's solution and the steady-state inactivation parameters of I_{Na} were quantitatively obtained in the presence or absence of 10 μM Rot. As shown in Fig. 1C, the normalized amplitude of I_{Na} was constructed against the conditioning potential and the smooth curves were well fitted by the Boltzmann equation as described in Materials and Methods. In control, $V_{1/2}$=-6.8±0.5 mV, k=6.2±0.4 (n=8), whereas in the presence of Rot (10 μM), $V_{1/2}$=-6.6±0.6 mV, k=6.3±0.5 (n=7). The values of neither $V_{1/2}$ nor slope factor (k) were noted to differ significantly between the absence and presence of 10 μM Rot. Therefore, the presence of Rot produced little or no modification on the inactivation curve of I_{Na} in these cells. Additionally, by use of nonlinear least-squares fit to the data points (Fig. 1E), the IC_{50} value needed to exert its inhibitory effect on peak I_{Na} amplitude was calculated to be 39.3 μM with a Hill coefficient of 1.2, and this agent at a concentration of 300 μM nearly abolished current amplitude.

Effect of Rot on Ca^{2+}-activated Cl^- current ($I_{Cl(Ca)}$) in mHippoE-14 cells

We next examined the effect of Rot on $I_{Cl(Ca)}$ in these cells. In these experiments, cells were immersed in normal Tyrode's solution and the recording pipette was filled with Cs^+-containing solution. Under the voltage profile applied, stepwise depolarizations produced

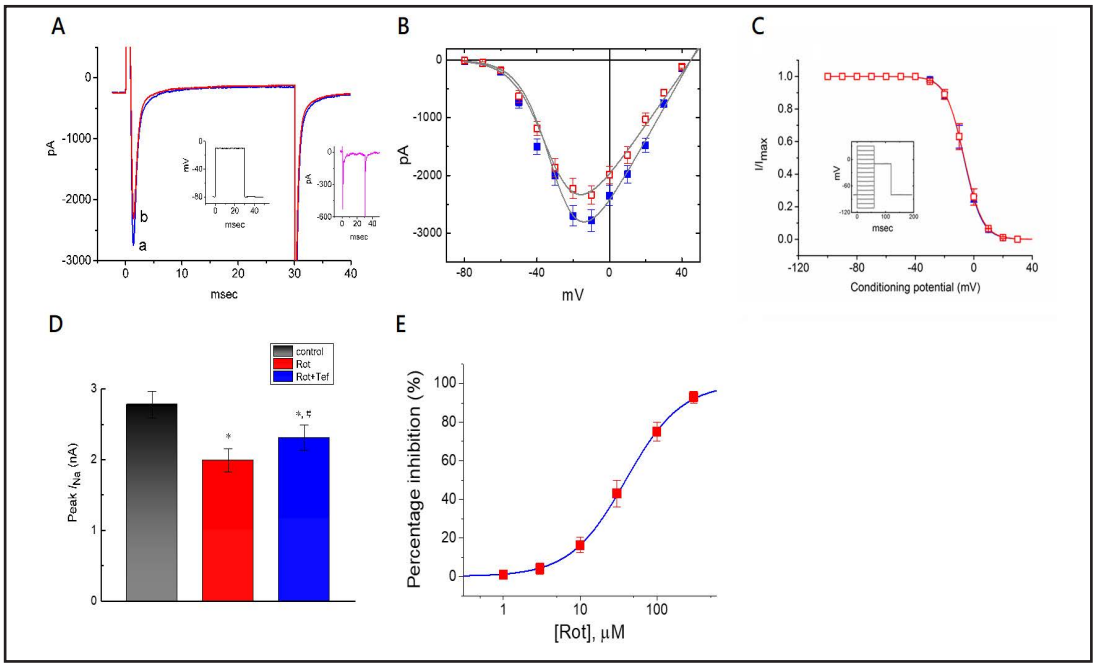

Fig. 1. Inhibitory effect of rotenone on I_{Na} in mouse hippocampal (mHippE-14) neurons. In this set of experiments, cells were bathed in Ca^{2+}-free Tyrode's solution containing 10 mM tetraethylammonium chloride and 0.5 mM $CdCl_2$. The recording pipette was filled with a Cs^+-containing solution. (A) Superimposed I_{Na} traces obtained in the absence (a) and presence (b) of 10 μM Rot. Inset in the middle of (A) indicates the voltage protocol used, while that in the right part is Rot-sensitive I_{Na} (i.e., the difference between traces a and b). (B) Averaged I-V relationships of peak I_{Na} in the absence (■) and presence (□) of 10 μM Rot (mean±SEM, n=7-9 for each point). The smooth gray curves taken with or without addition of Rot were fitted with a Boltzmann function as detailed in Materials and Methods. Note that the overall I-V relationship of this current remains unchanged in the presence of Rot, despite its ability to suppress I_{Na} amplitude. (C) Steady-state inactivation curve of I_{Na} obtained with or without addition of 10 μM rotenone (mean±SEM; n=6-8 for each point). Inset in (C) indicates the voltage profile used. Note that the inactivation curve of I_{Na} in the absence and presence of Rot is superimposed. (D) Bar graph showing effects of Rot and Rot plus tefluthrin on the peak amplitude of I_{Na}. Each cell was depolarized from -80 to -10 mV and peak I_{Na} was measured. In the experiments on Rot plus tefluthrin, tefluthrin was subsequently applied in continued presence of Rot. Each bar indicates the mean±SEM (n=8-11). Rot: 10 μM rotenone; Tef: 10 μM tefluthrin. *Significantly different from control ($P<0.05$) and #significantly different from Rot alone group ($P<0.05$). (E) Concentration-response curve for Rot-induced inhibition of peak I_{Na} in these cells. The peak amplitude of I_{Na} during cell exposure to Rot was compared with the control value (mean±SEM, n=7-12 for each point). The blue smooth line represents a best fit to a Hill function described in Materials and Methods. The values for IC_{50}, maximally inhibited percentage of peak I_{Na}, and the Hill coefficient were 39.3 μM, 100%, and 1.2, respectively.

a family of ionic currents which displayed both the slightly outward rectification and the slowing deactivating tail currents in response to a wide range of membrane potentials (Fig. 2). These currents, which tended to increase with time during the depolarizing step and to decay slowly with time following the return to holding potential, have been previously referred to as Ca^{2+}-activated Cl^- current ($I_{Cl(Ca)}$) [22, 23]. When cells were exposed to 10 μM Rot, the amplitude of $I_{Cl(Ca)}$ in response to membrane depolarization was progressively raised (Fig. 2). For example, when the cell was depolarized from -50 to +110 mV, the $I_{Cl(Ca)}$ amplitude measured at the end of voltage pulse was significantly increased to 681±96 pA (n=7, $P<0.05$) from a control of 230±61 pA. Likewise, the amplitude of slowly deactivating tail currents following the return to holding potential was also enhanced from to 223±17 to 427±25 pA (n=7, $P<0.05$). Furthermore, further addition of niflumic acid (1 μM), but still in the presence

of 10 μM Rot, effectively decreased deactivating $I_{Cl(Ca)}$ amplitude to 238±21 pA (n=5, P<0.05). Niflumic acid is recognized as a blocker of $I_{Cl(Ca)}$ [23]. As pipette solution contained 10 mM EGTA which strongly chelated free Ca^{2+}, addition of As the recording pipette was filled with 10 mM EGTA, in which intracellular Ca^{2+} was significantly reduced, addition of Rot (10 μM) failed to activated $I_{Cl(Ca)}$ in these cells.

The relationship between the Rot concentration and the amplitude of $I_{Cl(Ca)}$ was further

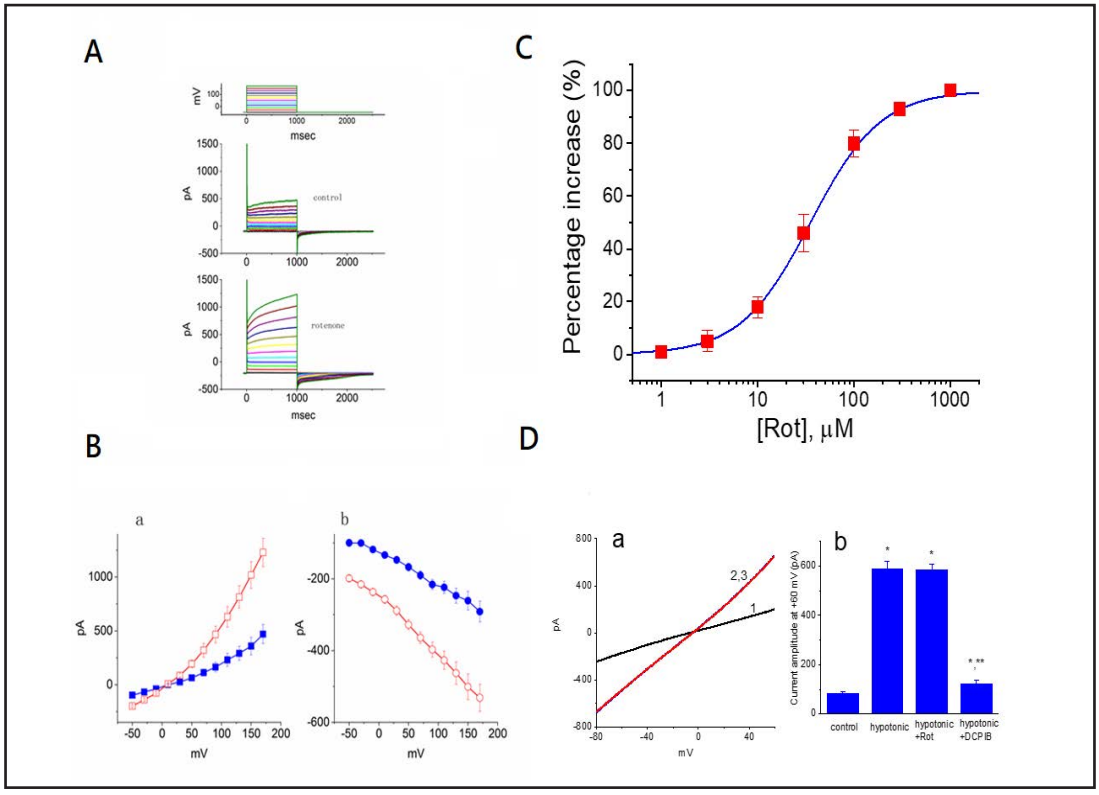

Fig. 2. Stimulatory effect of Rot on $I_{Cl(Ca)}$ in mHippE-14 cells. In these experiments, cells were bathed in normal Tyrode's solution containing 1.8 mM $CaCl_2$ and 10 mM tetraethylammonium chloride, and the recording pipettes used were filled with Cs^+-containing solution. The examined cells were held at -50 mV and the depolarizing pulses ranging from -50 to +170 mV that were increased in 20 mV increments were applied to the cell. (A) Superimposed $I_{Cl(Ca)}$ traces obtained in the absence (upper) and presence (lower) of 10 μM Rot. The uppermost part in (A) indicates the voltage protocol applied. (B) Averaged I-V relationship of $I_{Cl(Ca)}$ at the end of voltage pulses (a, square symbols) and the slowly deactivating tail current following return to the holding potential (b, circle symbols). The $I_{Cl(Ca)}$ amplitude was measured at the end of voltage pulse and the tail current upon repolarization was obtained after setting of capacitative current, usually between the tenth and twentieth millisecond after the end of voltage pulses. Filled symbols are controls and open symbols were taken during brief exposure to 10 μM Rot. Each point indicates the mean±SEM (n=9-11). (C) Concentration-response relationship for Rot-induced stimulation of $I_{Cl(Ca)}$. Each cell was depolarized from -50 to +100 mV with a duration of 1 sec and current amplitude at the end of depolarizing pulse was measured. The amplitude of $I_{Cl(Ca)}$ during exposure to 1 mM Rot was considered to be 100%. The smooth line represents the best fit to the Hill equation. The values for EC_{50} and the Hill coefficient were 35.4 μM and 1.2, respectively. Each point represents the mean±SEM (n=6-9). (D) Lack of effect of Rot on $I_{Cl(vol)}$ in mHippE-14 cells. (Ca) Superimposed current traces in response to ramp pulse from -80 to +60 mV with a duration of 1 sec. 1: control (i.e., isotonic solution); 2: hypotonic solution (200 mOsm); and 3 hypotonic solution plus 10 μM Rot. (Cb) Summary of data showing the effect of Rot or DCPIB on $I_{Cl(vol)}$ in response to hypotonic solution (200 mOsm) (mean±SEM, n=7 for each bar). Current amplitude was measured at the level of +60 mV. *Significantly different from control (i.e., isotonic solution) (P<0.05) and **significantly different from hypotonic solution alone (P<0.05).

evaluated. As illustrated in Fig. 2C, this compound (1 μM-1 mM) effectively increased the $I_{Cl(Ca)}$ amplitude in a concentration-dependent manner. The values of EC_{50} and Hill coefficient for Rot-stimulated $I_{Cl(Ca)}$ were calculated to be 35.4 μM and 1.2, respectively. Therefore, it is clear from these results that the presence of Rot is effective at activating the amplitude of $I_{Cl(Ca)}$ in mHippoE-14 cells. However, no change in volume-sensitive Cl^- current ($I_{Cl(vol)}$) was demonstrated in the presence of 10 μM Rot, although addition of DCPIB (10 μM), a blocker of $I_{Cl(vol)}$, significantly suppressed the amplitude of $I_{Cl(Vol)}$ (Fig. 2D).

K_{ATP}-channel activity of mHippoE-14 cells caused by the presence of Rot

Rot was previously reported to induce a tolbutamide-sensitive outward current in nigral dopaminergic neurons [4]. The activity of K_{ATP} channels present in mHippoE-14 cells was further investigated with or without addition of Rot. In this series of experiments, mHippoE-14 cells were bathed in Ca^{2+}-free Tyrode's solution. In cell-attached configuration, each cell examined was held at the level of -60 mV relative to the bath. As in the experiment of Fig. 3, when Rot at a concentration of 10 μM was applied to the bath, K_{ATP}-channel activity was progressively increased (Fig. 3A). The K_{ATP}-channel currents occurred in rapid open-closed transitions and in brief bursts with single-channel amplitude of 2.71±0.08 (n=8) at -60 mV. The presence of Rot (10 μM) significantly increased the probability of channel openings from 0.007±0.0008 to 0.012±0.001 (n=8, $P<0.05$). However, on the basis of mean-variance analysis for single K_{ATP} channels in these cells, no significant difference in single-channel amplitude between the absence and presence of Rot was demonstrated (Fig. 3C). There was no detectable difference in the amplitude of single K_{ATP} channels between the absence and presence of 10 μM Rot (2.69±0.09 pA [control] versus 2.71±0.08 pA [Rot], n=8, $P>0.05$). Moreover, tolbutamide (10 μM), if Rot (10 μM) was still present, caused a reduction of channel activity to 0.009±0.0008 (n=6, $P<0.05$); however, in continued presence of Rot, further addition of 4, 4'-dithiodipyridine did not increase the channel open probability further. 4, 4'-Dithiodipyridine was previously reported to activate K_{ATP} channels in pituitary GH_3 lactotrophs [24]. The K_{ATP}-channel activity at various membrane potentials was also examined in the presence of Rot. The plot of single-channel amplitude as a function of holding potential was constructed. Fig. 3D illustrates the averaged *I-V* relation of single-channel currents during the exposure to Rot (10 μM). However, in inside-out configuration, addition of Rot to the bath was found to produce minimal effects on the activity of K_{ATP} channels in mHippoE-14 cells.

The activity of MEPPs in the absence and presence of Rot recorded from mHippoE-14 cells

Whether Rot produces any effects on the activity of MEPPs recorded from mHippoE-14 cells was further investigated in another set of experiments. Cells were bathed in normal Tyrode's solution containing 1 μM tetrodotoxin. Tetrodotoxin blocked the presence of spontaneous electrical firing on which MEPPs could be overlaid. Under current-clamp condition, autaptic activity with MEPPs at a frequency of about 1 Hz was clearly observed. Under our experimental conditions as described previously [25-27], synapses tend to be appropriately formed by autaptic mHippE-14 neurons. When cells were exposed to Rot at a concentration of 3 and 10 μM, neither the MEPPs amplitude nor the values of rise and decay tau were significantly changed (Table 2); however, the presence of Rot did raise the frequency of MEPPs significantly (Fig. 4). Addition of MK-801 (100 μM), still in the presence of 10 μM Rot, significantly decreased Rot-induced increase of MEPP frequency. Moreover, the resting potential with or without addition of Rot (10 μM) was noted to be not changed significantly (69.5±1.6 mV [n=9; control] versus 69.7±1.9 mV [n=8; Rot], $P>0.05$). Likewise, when whole-cell voltage clamp mode was made, the activity of autaptic currents was found to be enhanced in the presence of 10 μM Rot (Fig. 5A). A leftward shift in the relationship of cumulative probability versus inter-event interval was seen during the exposure to 10 μM Rot (Fig. 5B); however, the cumulative probability of current amplitude remained unchanged. The results prompted us to suggest that the increase of MEPP frequency after addition of Rot is not due to cell depolarization, despite its ability to increase MEPP frequency.

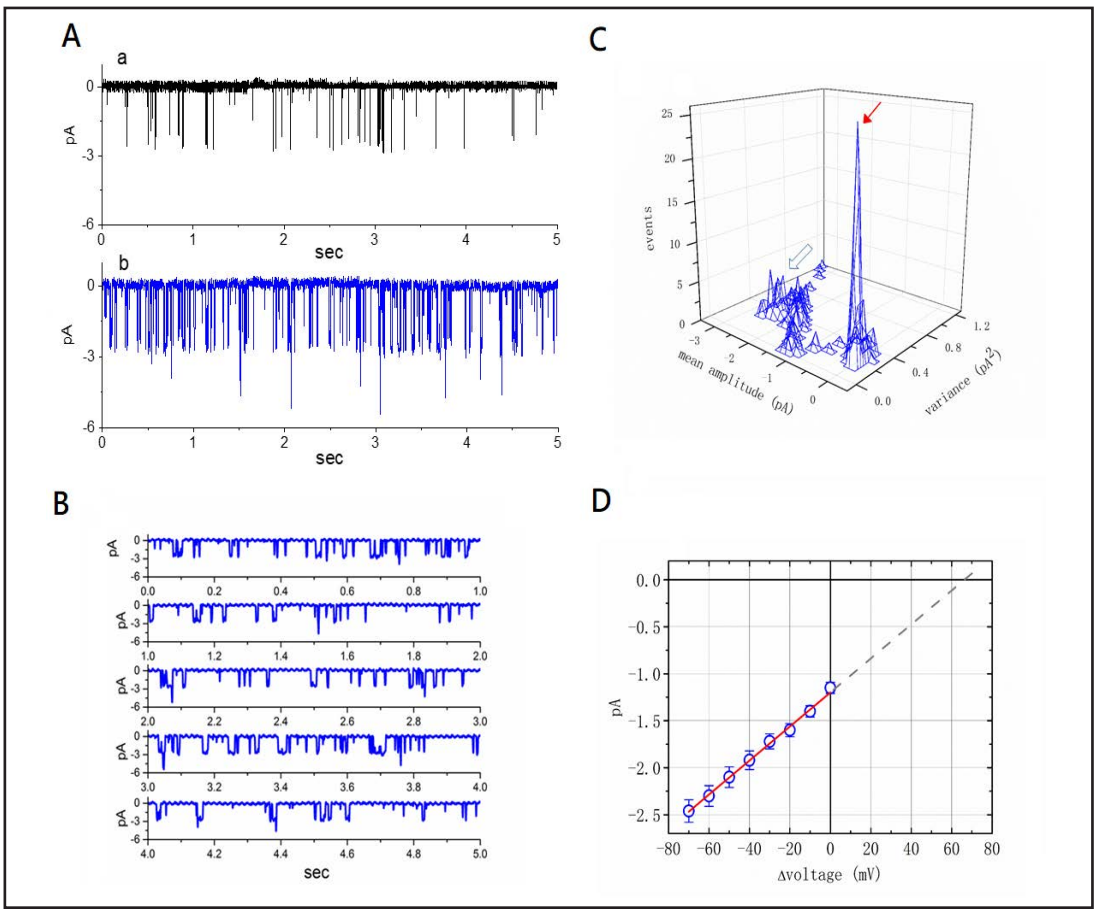

Fig. 3. Stimulatory effect of Rot on the activity of K_{ATP} channels in mHippoE-14 cells. Single channel recordings were made under cell-attached configuration and cells were immersed in Ca^{2+}-free Tyrode's solution. (A) Original K_{ATP}-channel current measured at -60 mV relative to the bath in the absence (a) and presence (b) of 10 μM Rot. K_{ATP}-channel opening gives a downward deflection in current. Current trace in panel (B) indicates an expanded record from panel (Ab). (C) Mean variance histogram of K_{ATP} channel obtained in the presence of 10 μM Rot. Open arrow shown in (C) denotes one open level with mean current of -2.7 pA, while the closed state corresponds to the peak at 0 pA indicated by red arrow. (D) Averaged I-V relationship of single K_{ATP}-channel currents (mean±SEM; n=7-9 for each point). The broken line is pointed toward the value of the reversal potential with +67 mV. The linear I-V relationship of K_{ATP} channels in the presence of 10 μM Rot shows the single-channel conductance of approximately 18.1 pS.

Simulated bursting pattern of APs in XC modeled neuron with varying g_{aut}

In a final set of study, we explored how the dynamics of bursting firing in a modeled neuron can be altered by increasing the values of g_{aut} to mimic the effects of Rot on I_{aut} described above. The descriptions for this modeled neuron were detailed previously [16, 17] and an autaptic synapse with varying strength was incorporated into the model [18, 19]. The g_{aut} value reflects the autaptic self-feedback strength and other default parameters are

Table 2. Parameter values of MEPPs obtained with or without addition of Rot. *Significantly different from control (P<0.05)

	Control	Rot (3 μM)	Rot (10 μM)
Cell number	8	7	7
Rise tau (msec)	55.4 ± 2.2	54.8 ± 2.3	54.7 ± 2.2
Decay tau (msec)	206 ± 11	207 ± 13	207 ± 15
Peak amplitude (mV)	4.9 ± 0.2	5.0 ± 0.3	5.1 ± 0.3
Mean frequency (Hz)	0.93 ± 0.12	1.36 ± 0.18*	1.56 ± 0.21*

illustrated in Table 1. For studying this, a brief depolarizing current with 0.02 mA/cm^2 was applied to modeled central neuron (i.e., XC modeled neuron), in an attempt to generate bursting firing of neuronal APs. It is clear from these simulations that the delayed autaptic feedback connection greatly modifies the response dynamics of the modeled neuron. The structure of the interspike intervals of the bursting patterns of a modeled neuron in response to varying g_{aut} is illustrated in Fig. 6A. The varying spike frequency of burst firing in response to different values of g_{aut} was detected in a periodical fashion. There was a progressive shortening of the interspike interval (i.e., the interval of intraburst APs over time) in combination with to facilitate the transition toward chaotic bursting, particularly when the g_{aut} value was greater than 1 mS/cm^2. Moreover, by elevating g_{aut} value to 0.1 and 0.5 mS/cm^2 to mimic the action of Rot (3 and 10 μM), we were able to show an increase in intrabursting firing and the emergence of subthreshold potentials (Fig. 6B).

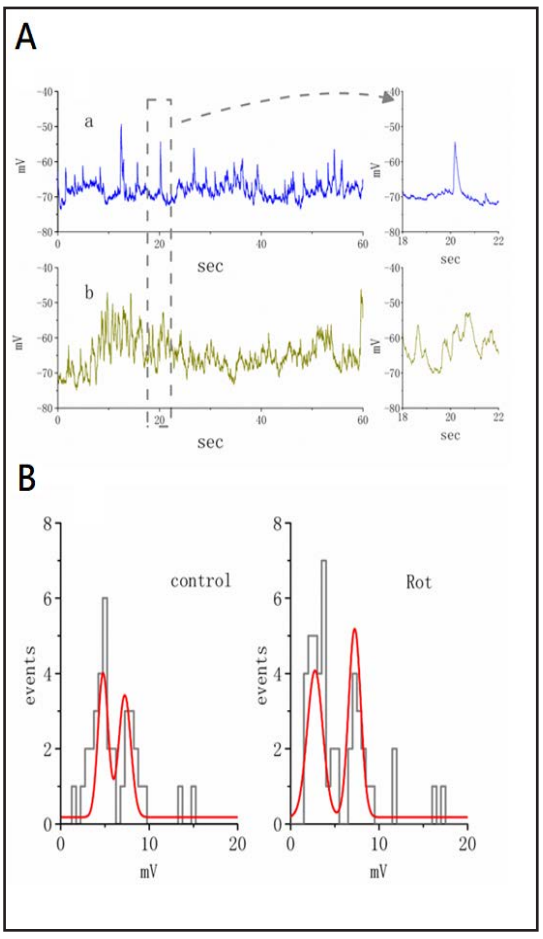

Fig. 4. Effect of Rot on MEPPs recorded from mHippoE-14 cells. Cells were bathed in normal Tyrode's solution containing 1.8 mM $CaCl_2$ and 1 μM tetrodotoxin. (A) Potential traces obtained in the absence (a) and presence (b) of 10 μM Rot. The right sides in (A) indicate expanded records from dashed box in left side. (B) Amplitude histogram of MEPPs obtained in control (left) and after addition of 10 μM Rot (right). The red smooth lines in each panel were well fit by multi-gaussian function.

Discussion

This study provides the evidence to show that Rot can exert multiple actions on ion currents inherently in mHippoE-14 hippocampal neurons. A current study reported the ability of Rot to enhance the amplitude of L-type Ca^{2+} current in vascular A7r5 myocytes with a hyperpolarizing shift of *I-V* relationship of this current [8]. However, distinguishable from that, our results demonstrated that addition of Rot decreased the peak amplitude of I_{Na} in mHippoE-14 cells in a concentration-dependent fashion, although no significant change in the steady-state inactivation curve of peak I_{Na} was change in the presence of Rot. As cells were exposed to Rot, neither activation nor inactivation time course of peak I_{Na} was altered. Moreover, tefluthrin, still in the presence of Rot, can reverse the inhibition by this compound of peak I_{Na}. Although the discrepancy of these results is unclear, it could be due to different types of cells examined. It is also possible that the I_{Na} and Ca^{2+} currents tend to be differentially regulated by Rot and that Rot-induced inhibition of I_{Na} is associated with its production of reactive oxygen species [4].

The IC_{50} value required for Rot-mediated inhibition of peak I_{Na} is about 39.3 μM. Because the pipette solution used in our whole-cell recordings contained a constant level of pH and ATP, it seems unlikely that Rot-induced suppression of peak I_{Na} is linked to changes in either intracellular pH or ATP content. It is also tempting to speculate that the α-subunit of the $Na_V1.1$ or $Na_V1.6$ channels, which are respectively encoded by the *SCN1A* or *SCN8A* gene, is functionally expressed in mHippoE-14 cells [16, 28].

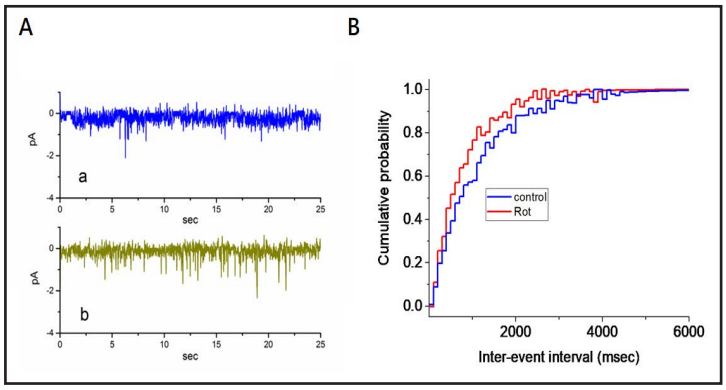

Fig. 5. The activity of autaptic currents recorded from mHippoE-14 cells. Cells were bathed in normal Tyrode's solution containing 1 μM tetrodotoxin. Tetrodoxin was used to block spontaneous firing of neuronal action currents which reflect the occurrence of APs. In (A), under whole-cell voltage-clamp configuration, a cell was held at -70 mV and current amplitude was measured in the absence (a) and presence (b) of 10 μM Rot. Note that the downward deflection indicates the activity of autaptic inward currents. (B) Relationship of cumulative probability versus inter-event interval. Note that there was a leftward shift in the cumulative probability of autaptic currents in the presence of 10 μM Rot.

The $I_{Cl(Ca)}$ is functionally expressed in a subset of neurons used for performing a specific function for this subset of neurons [22]. The magnitude of $I_{Cl(Ca)}$ in hippocampal neurons is involved in AP repolarization, generation of after-polarizations, and membrane oscillatory behavior [22, 29]. Our study also found out that Rot can enhance the amplitude of $I_{Cl(Ca)}$ in mHippoE-14 cells with an EC_{50} value of 35.4 μM. However, in the continued presence of Rot, further application of nimodipine did not reversed the $I_{Cl(Ca)}$ amplitude activated by Rot. It thus seems unlikely that Rot-mediated stimulation of $I_{Cl(Ca)}$ in mHippoE-14 cells is closely associated with changes in the amplitude of L-type Ca^{2+} current, although the detailed mechanism of Rot-induced stimulatory action on $I_{Cl(Ca)}$ remains to be studied. It is likely that the functional expression of TMEM16A, TMEM16B, or both [29], combines to contribute to generation of $I_{Cl(Ca)}$ in mHippoE-14 cells.

The single-channel conductance of K_{ATP} channels in mHippoE-14 cells was 18.1±0.3 pS (n=9). This value is similar to those of typical K_{ATP} channels reported in certain types of neurons, but lower than that of K_{ATP} channels seen in endocrine cells [24]. Previous reports have shown that the Kir6.2/SUR1 complex tends to be the best candidate for the brain function K_{ATP} channels [30]. On the basis of biophysical and pharmacological properties, the K_{ATP} channel in mHippoE-14 cells appears to be distinguished from those in hippocampal

Fig. 6. Effects of changes in g_{aut} on the bursting pattern of APs in modeled hippocampal neuron adapted from Xu and Clancy [16]. (A) Bifurcation diagram of the interspike interval (ISI) of modeled neuron with a chemical autapse versus varying autaptic conductance. The delayed time and external stimulus were arbitrarily set at 5 msec and 0.02 mA/cm^2, respectively. (B) Simulated firing of bursting APs generated from model neuron to mimic the effect of Rot. The g_{aut} values in panels a, b and c are 0, 0.1 and 0.5 mS/cm^2, respectively. Traces (a) is simulated at g_{aut}=0 mS/cm^2, whereas traces (b) and (c) are arbitrarily set to mimic the action of Rot at a concentration of 3 and 10 μM, respectively.

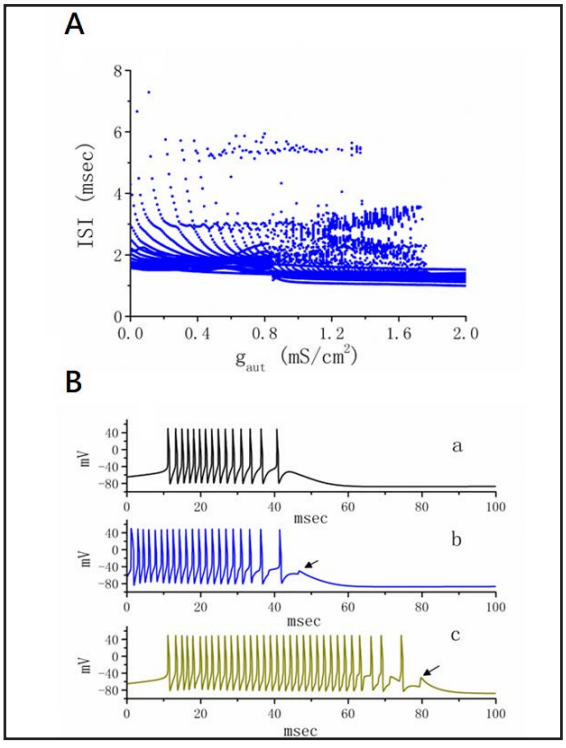

H19-7 neurons and other types of neurons [13, 14, 30, 31]. It is thus likely that Kir6.1 was functionally expressed in mHippoE-14 cells. It remains to be further determined whether K_{ATP} channels in mHippoE-14 cells are heteromers composed of SUR and Kir6.1 subunits. Nonetheless, the activity of K_{ATP} channels in hippocampal neurons would be highlighted for either ischemic insults or epileptic activity during hyperglycemic state [31-33].

Rot-induced activity of K_{ATP} channels was clearly observed in mHippoE-14 cells. 4, 4'-Dithiodipyridine did not increase channel activity further; however, tolbutamide was effective at suppressing Rot-mediated channel activity. Moreover, in inside-out configuration, addition of Rot to the bath had no effects on the probability of K_{ATP}-channel openings. Consistent with previous observations [34], the results can be primarily explained by the ability of Rot to induce overproduction of reactive oxygen species accumulated inside the cell.

In our study, we found that addition of Rot to mHippoE-14 cells increased the frequency of MEPPs. Subsequent addition of MK-801 was effective at reversing Rot-mediated increase of MEPPs frequency. It is thus possible that mHippoE-14 cells contain high concentrations of glutamate, and readily form synapses onto itself which have been identified as an autaptic culture system [26]. Under such synapse pairs, effective contact is signaled by the emergence of MEPPs. It has been demonstrated that Rot reduced paired-pulse ratios at mossy fiber-CA3 synapses, indicating increased neurotransmitter release probabilities and exacerbates seizures [35]. Nonetheless, the mHippoE-14 cells in culture (i.e., autaptic cultures) tend to be electrically or chemically coupled and may provide a simple system to elucidate the mechanism of receptor-evoked neurotransmitter secretion, the presynaptic release machinery, or both, because of a reduced model system which displays less interaction by other inputs or by feed-back regulations [18, 19, 25-27, 36, 37].

Rot has been previously reported to potentiate NMDA-induced currents in substantia nigra dopaminergic neurons [7]. However, in our study, no detectable changes in MEPP amplitude and the time course of rise and decay were demonstrated in the presence of Rot, although it did enhance MEPP frequency. It seems unlikely that Rot itself effected any change in NMDA receptors in mHippoE-14 cells. Moreover, in our theoretical study, the autaptic conductance was incorporated to XC modeled neuron in attempts to mimic the Rot action on central neuron. When the strength of autaptic coupling was increased, the bursting frequency of neuronal APs was increased and the transition to chaotic bursting was facilitated. Therefore, through its effects on MEPPs and autaptic activity, bursting patterns are expected to be greatly altered.

In conclusion, Rot was able to suppress the amplitude of I_{Na} and to enhance $I_{Cl(Ca)}$ and the activity of K_{ATP} channels, and it increased the frequency of MEPPs. Rot-mediated increase of $I_{Cl(Ca)}$ may cause membrane depolarization, thereby enhancing neuronal excitability. However, such depolarization could be reversed by its activation of K_{ATP} channels and the increased excitability tends to be depressed by its suppression of I_{Na}. Taken together, the cellular electrophysiological effects of Rot on membrane ion currents inherently in mHippoE-14 cells might significantly contribute to its neurotoxic actions *in vivo* [38].

Abbreviations

AP (action potential); BK_{Ca} (channel, large-conductance Ca^{2+}-activated K^+ channel); DCPIB (4-[(2-butyl-6, 7-dichloro-2-cyclopentyl-2, 3-dihydro-1-ox-1H-inden-5-yl)oxy] butanoic acid); EC_{50} (a 50% stimulation of $I_{Cl(Ca)}$); g_{aut} (autaptic conductance); I_{aut} (autaptic current); IC_{50} (a 50% inhibition of peak I_{Na}); $I_{Cl(Ca)}$, Ca^{2+}-activated (Cl^- current); $I_{Cl(vol)}$, volume-sensitive (Cl^- current); I_{Na} (voltage-gated Na^+ current); ISI (interspike interval); *I-V* (current versus voltage); MEPP (miniature end-plate potential); Rot (rotenone); SEM (standard error of the mean); K_{ATP} (channel, ATP-sensitive K^+ channel); Xu-Clancy (model, XC model).

Acknowledgements

This study was partly funded by National Cheng Kung University (D104-35A16 to S.N. Wu), National Cheng Kung University Hospital (20180254 to C.W. Huang), Kaohsiung Chang Gung Memorial Hospital (CMRPG8D0122 to Y.C. Chuang), and Ministry of Science and Technology (103-2314-B-182A-029-MY3 to Y.C. Chuang, 106-2314-B-006-034 and 106-2320-B-006-055 to C.W. Huang), Taiwan. The authors acknowledge Hui-Zhen Chen and Huei-Ting Su for parts of the experiments.

Disclosure Statement

No conflicts of interests, financial or otherwise, are declared by the authors.

References

1 Gao HM, Liu B, Zhang W, Hong JS: Novel anti-inflammatory therapy for Parkinson's disease. Trends Pharmacol Sci 2003;24:395-401.
2 Fato R, Bergamini C, Bortolus M, Maniero AL, Leoni S, Chnishi T, Lenaz G: Differential effects of mitochondrial Complex I inhibitors on production of reactive oxygen species. Biochim Biophys Acta 2009;1787:384-392.
3 Gao XF, Wang W, He C. Rotenone inhibits delayed rectifier K^+ current via a protein kinase A-dependent mechanism. Neuroreport 2008;19:1401-1405.
4 Freestone PS, Chung KK, Guatteo E, Mercuri NB, Nicholson LF, Lipski J. Acute action of rotenone on nigral dopaminergic neurons—involvement of reactive oxygen species and disruption of Ca^{2+} homeostasis. Eur J Neurosci 2009;30:1849-1859.
5 Dong L, Xie MJ, Zhang P, Ji LL, Liu WC, Dong MQ, Gao F. Rotenone partially reverses decreased BK_{Ca} currents in cerebral artery smooth muscle cells from streptozotocin-induced diabetic mice. Clin Exp Pharmacol Physiol 2009;36:e57-e64.
6 Nazıroğlu M, Özgül C, Çiğ B, Doğan S, Uğuz AC. Glutathione modulates Ca^{2+} influx and oxidative toxicity through TRPM2 channel in rat dorsal root ganglion neurons. J Membr Biol 2011;242:109-118.
7 Wu YN, Johnson SW: Rotenone potentiates NMDA currents in substantia nigra dopamine neurons. Neurosci Lett 2007;421:96-100.
8 Ochi R, Dhagia V, Lakhkar A, Patel D, Wolin MS, Gupte SA: Rotenone-stimulated superoxide release from mitochondrial complex I acutely augments L-type Ca^{2+} current in A7r5 aortic smooth muscle cells. Am J Physiol Heart Circ Physiol 2016;310:H1118-1128.
9 Gingerich S, Kim GL, Chalmers JA, Koletar MM, Wang X, Wang Y, Belsham DD: Estrogen receptor alpha and G-protein coupled receptor 30 mediate the neuroprotective effects of 17β-estradiol in novel novel murine hippocampal cell models. Neuroscience 2010;170:54-56.
10 Lazniewska J, Milowska K, Zablocka M, Mignani S, Caminade AM, Majoral JP, Bryszewska M, Gabryelak T. Mechanism of cationic phosphorus dendrimer toxicity against murine neural cell lines. Mol Pharm 2013;10:3484-3496.
11 Evans NJ, Bayliss AL, Reale V, Evans PD: Characterization of signalling by the endogenous GPER1 (GPR30) receptor in an embryonic mouse hippocampal cell line (mHippoE-18). PLoS One 2016;11:e0152138.
12 Milowska K, Szwed A, Zablocka M, Caminade AM, Majoral JP, Mignani S, Gabryelak T, Bryszewska M: In vitro PAMAM, phosphorus and viologen-phosphorus dendrimers prevent rotenone-induced cell damage. Int J Pharm 2014;474:42-49.
13 Huang CW, Huang CC, Liu YC, Wu SN: Inhibitory effect of lamotrigine on A-type potassium current in hippocampal neuron-derived H19-7 cells. Epilepsia 2004;45:729-736.
14 Huang CW, Huang CC, Wu SN: The opening effect of pregabalin on ATP-sensitive potassium channels in differentiated hippocampal neuron-derived H19-7 cells. Epilepsia 2006;47:720-726.
15 Wu SN, Lin PH, Hsieh KS, Liu YC, Chiang HT: Behavior of nonselective cation channels and large-conductance Ca^{2+}-activated K^+ channels induced by dynamic changes in membrane stretch in cultured smooth muscle cells of human coronary artery. J Cardiovasc Electrophysiol 2003;14:44-51.

16 Xu J, Clancy CE: Ionic mechanisms of endogenous bursting of CA3 hippocampal pyramidal neurons: a model study. PLoS One 2008;3:e2056.
17 Hsu HT, Tseng YT, Lo YC, Wu SN: Ability of naringenin, a bioflavonoid, to activate M-type potassium current in motor neuron-like cells and to increase BK_{Ca}-channel activity in HEK293T cells transfected with α-hSlo subunit. BMC Neurosci 2014;15:135.
18 Wang H, Ma J, Chen Y, Chen Y: Effect of an autapse on the firing pattern transition in a bursting neuron. Commun Nonlinear Sci Numer Simulat 2014;19:3242-3254.
19 Wang H, Wang L, Chen Y, Chen Y: Effect of autaptic activity on the response of a Hodgkin-Huxley neuron. Chaos 2014;24:033122.
20 Wu SN, Wu YH, Chen BS, Lo YC, Liu YC: Underlying mechanism of actions of tefluthrin, a pyrethroid insecticide, on voltage-gated ion currents and on action currents in pituitary tumor (GH_3) cells and GnRH-secreting (GT1-7) neurons. Toxicology 2009;258:70-77.
21 He B, Soderlund DM: Effects of the 1 auxiliary subunit on modification of rat Nav1.6 sodium channels expressed in HEK293 cells by the pyrethroid insecticides tefluthrin and deltamethrin. Toxicol Appl Pharmacol 2016;291:58-69.
22 Hartzell C, Putzier I, Arreola J: Calcium-activated chloride channels. Annu Rev Physiol 2005;67:719-758.
23 Hawkins EG, Dewey WL, Anitha M, Srinivasan S, Grider JR, Akbarali HL: Electrophysiological characteristics of enteric neurons isolated from the immortomouse. Dig Dis Sci 2013;58:1516-1527.
24 Wu SN, Li HF, Chiang HT: Characterization of ATP-sensitive potassium channels functionally expressed in pituitary GH_3 cells. J Membr Biol 2000;178:205-214.
25 Saada R, Miller N, Hurwitz I, Susswein AJ: Autaptic excitation elicits persistent activity and a plateau potential in a neuron of known behavioral function. Curr Biol 2009;19:479-484.
26 Rost BR, Breustedt J, Schoenherr A, Grosse G, Ahnert-Hilger G, Schmitz D: Autaptic cultures of single hippocampal granule cells of mice and rats. Eur J Neurosci 2010;32:939-947.
27 Burgalossi A, Jung SY, Man KM, Nair R, Jockusch WJ, Wojcik SM, Brose N, Rhee JS: Analysis of neurotransmitter release mechanisms by photolysis of caged Ca^{2+} in an autaptic neuron culture system. Nat Protoc 2012;7:1351-1365.
28 Akin EJ, Solé L, Johnson B, Beheiry ME, Masson JB, Krapf D, Tamkun MM. Single-molecule imaging of Nav1.6 on the surface of hippocampal neurons reveals somatic nanoclusters. Biophys J 2016;111:1235-1247.
29 Huang WC, Xiao S, Huang F, Harfe BD, Jan YN, Jan LY: Calcium-activated chloride channels (CaCCs) regulate action potential and synaptic response in hippocampal neurons. Neuron 2012;74:179-192.
30 Betourne A, Bertholet AM, Labroue E, Halley H, Sun HS, Lorsignol A, Feng ZP, French RJ, Penicaud L, Lassalle JM, Frances B: Involvement of hippocampal CA3 K_{ATP} channels in contextual memory. Neuropharmacology 2009;56:615-625.
31 Chen BS, Wu SN: Functional role of the activity of ATP-sensitive potassium channels in electrical behavior of hippocampal neurons: experimental and theoretical studies. J Theor Biol 2011;272:16-25.
32 Huang CW, Wu SN, Cheng JT, Tsai JJ, Huang CC: Diazoxide reduces status epilepticus neuron damage in diabetes. Neurotox Res 2010;17:305-316.
33 Huang CW, Lai MC, Cheng JT, Tsai JJ, Huang CC, Wu SN: Pregabalin attenuates excitotoxicity in diabetes. PLoS One 2013;8:e65154.
34 Satish Bollimpelli V, Kondapi AK: Differential sensitivity of immature and mature ventral mesencephalic neurons to rotenone induced neurotoxicity *in vitro*. Toxicol In Vitro 2015;30:545-551.
35 Simeone KA, Matthews SA, Samson KK, Simeone TA: Targeting deficiencies in mitochondrial respiratory complex I and functional uncoupling exerts anti-seizure effects in a genetic model of temporal lobe epilepsy and in a model of acute temporal lobe seizures. Exp Neurol 2014;251:84-90.
36 Liu H, Dean C, Arthur CP, Dong M, Chapman ER: Autapses and networks of hippocampal neurons exhibit distinct synaptic transmission phenotypes in the absence of synaptotagmin I. J Neurosci 2009;29:7395-7403.
37 Wu Y, Gong Y, Wang Q: Autaptic activity-induced synchronization transitions in Newman-Watts network of Hodgkin-Huxley neurons. Chaos 2015;25:043113.
38 Darbinyan LV, Hambardzumyan LE, Simonyan KV, Chavushyan VA, Manukyan LP, Sarkisian VH. Rotenone impairs hippocampal neuronal activity in a rat model of Parkinson's disease. Pathophysiology 2017;24:23-30.